

Supporting Information

Enhancing the dispersion of Cu-Ni metals on graphene aerogel support for use as a catalyst in the direct synthesis of dimethyl carbonate from carbon dioxide and methanol

Varisara Deerattrakul, Apichaya Panitprasert, Pralachoak Puengampholsrisook, Paisan Kongkachuichay

Department of Chemical Engineering, Faculty of Engineering, and Research Network of NANOTEC-KU on NanoCatalysts and NanoMaterials Sustainable Energy and Environment, Kasetsart University, Bangkok 10900, Thailand

In addition to the Cu-Ni/graphene aerogel catalyst, bare graphene aerogel was characterized by various techniques including SEM, TEM, XRD, Raman, XPS, and N₂ sorption, which are described in this section. The morphology of graphene aerogel (G_{aero}) was characterized by FE-SEM and TEM as shown in Figure S1. FE-SEM image of graphene aerogel (Figure S1a) shows interconnected porous structure attributing to the large enterable area of graphene and providing abundant porous architectures due to the intermolecular force of π - π conjugation of graphene nanosheets¹. As shown in Figure S1b, TEM image of graphene aerogel displays almost transparent sheets with many wrinkles, resulting from their interconnected 3D frameworks structures.

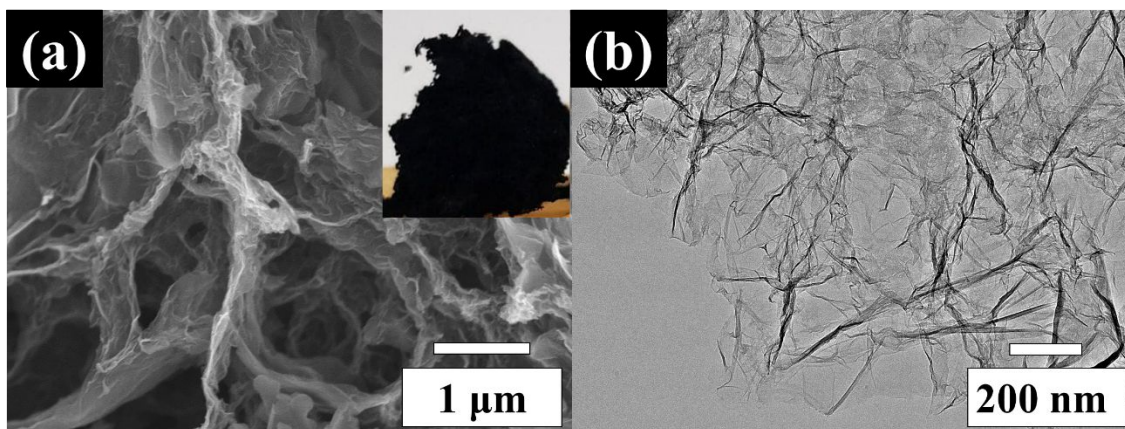


Figure S1. (a) FE-SEM and (b) TEM images of graphene aerogel.

XRD analysis shown in Figure S2a displays the crystallographic structure of graphene aerogel and graphite oxide (GO). The main peak of GO exhibits a sharp peak at around 10° related to the (001) reflection, which is attributed to the crystallinity of aligned GO due to the oxygen functionality². After reduction process, the main peak of GO at 10° completely disappeared and shifted to around 25° related to (002) plane indicating the efficient reduction of GO to graphene aerogel^{3,4}. To further clarify the surface chemical composition of graphene aerogel and GO (Figure S2b), XPS spectra of all samples show only C1s and O1s peaks confirming that there are no any impurities. Notably, the O1s peak of graphene aerogel significantly decreased in intensity because the oxygen-containing functional groups of GO were removed during the hydrothermal reduction, which is in agree with XRD results. To identify the quality of graphene-based supports, the Raman spectra of all samples (see Figure S2c) display two remarkable peaks at around 1356 cm^{-1} and 1597 cm^{-1} , representing to the D band and the G band, respectively. It is generally known that D band is related to the disordered carbon structure (sp^3) with the breathing mode of k-point phonons of A_{1g} symmetry, while G band is correlated

with sp^2 carbon structure (the E_{2g} mode) ⁵. Additionally, the intensity ratio of the D band to G band (I_D/I_G) increases when the defect degree of graphitization increases ^{6, 7}; therefore, the I_D/I_G values of GO and graphene aerogel are 0.85 and 1.0, respectively, indicating that GO was successfully reduced to graphene aerogel.

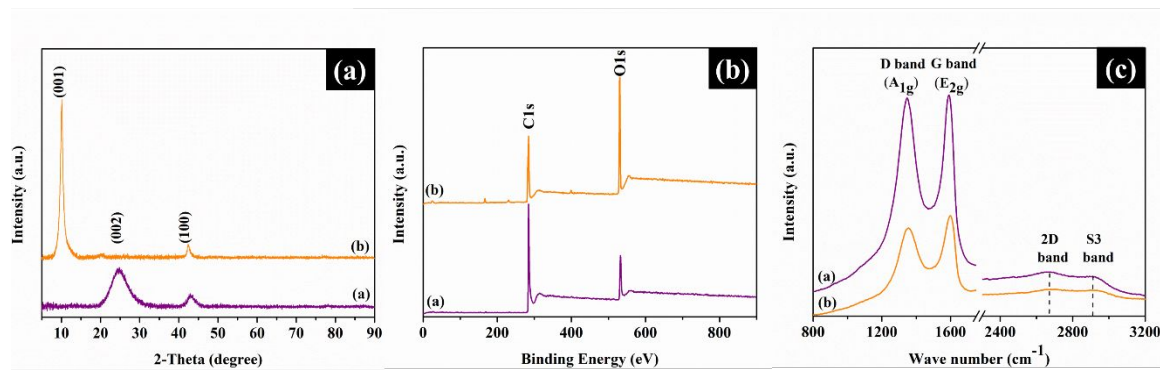


Figure S2. (a) XRD patterns, (b) survey XPS spectra, and (c) Raman spectra of samples [Note that (a) and (b) symbols in Fig. S2a–c are graphene aerogel and GO, respectively].

The N_2 sorption isotherm of graphene aerogel (Figure S3) is assigned to a type-IV isotherm (H3-type hysteresis loop), owing to the porous 3D framework ⁸. Moreover, the BET surface area shows that graphene aerogel has a specific surface area of $421 \text{ m}^2 \text{ cm}^{-1}$ and the pore size distribution displays the main peaks at around 2.44, 3.41, and 5.60 nm, corresponding to the mesoporous structures. As all evidence above, it is concluded that graphene aerogel was successfully synthesized *via* simply hydrothermal reduction method.

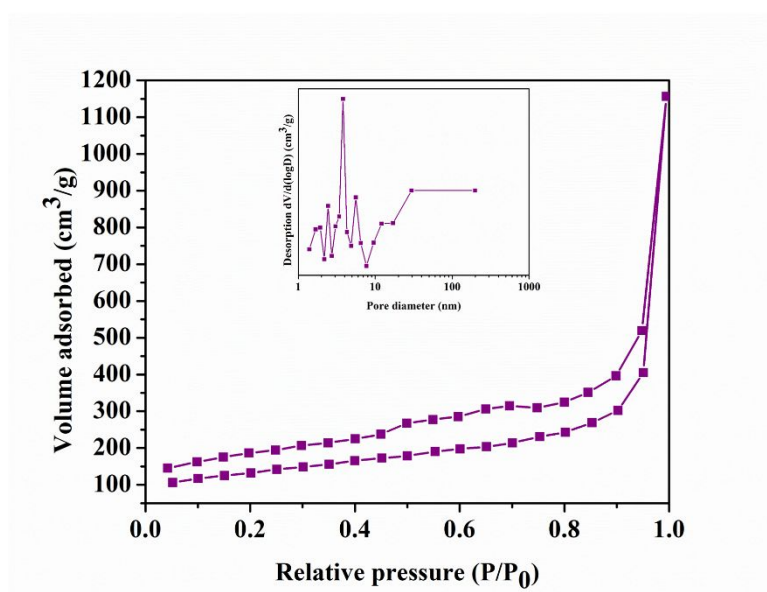


Figure S3. N₂ sorption isotherm of graphene aerogel.

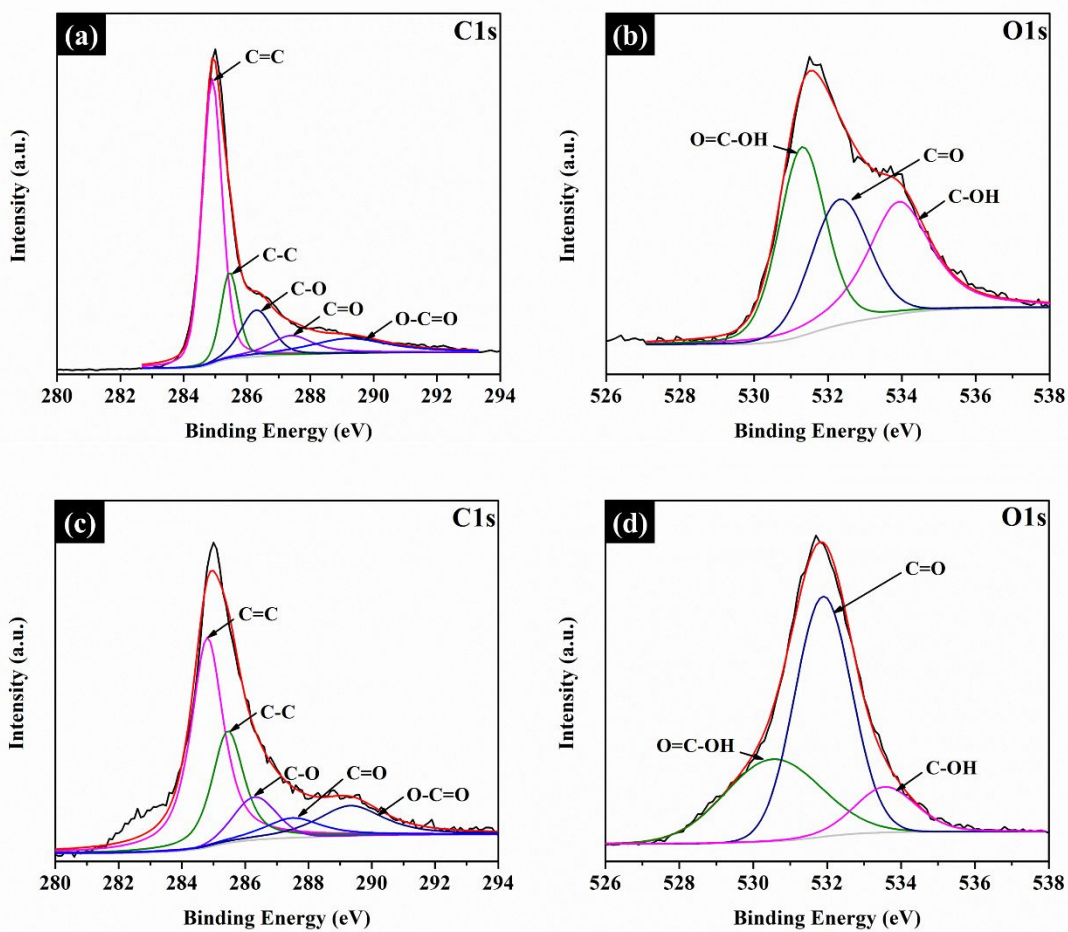


Figure S4. C1s XPS spectra of 15%Cu-Ni/graphene aerogel: (a) route A and (c) route B and O1s XPS spectra of 15%Cu-Ni/graphene aerogel: (b) route A and (d) route B.

Table S1. Metal contents of Cu-Ni/graphene aerogel after loading Cu-Ni simultaneously with hydrothermal reaction of graphene oxide (determined by ICP-OES).

Sample	Cu content (wt.%)	Ni content (wt.%)
10%Cu-Ni/graphene aerogel	3.45	0.55
15%Cu-Ni/graphene aerogel	3.47	0.62
20%Cu-Ni/graphene aerogel	5.22	1.14
25%Cu-Ni/graphene aerogel	5.60	1.20

REFERENCES

- (1) Li, Y.; Cui, W.; Liu, L.; Zong, R.; Yao, W.; Liang, Y.; Zhu, Y. Removal of Cr(VI) by 3D TiO₂-Graphene Hydrogel via Adsorption Enriched with Photocatalytic Reduction. *Appl. Catal. B* **2016**, *199*, 412–423.
- (2) Ren, Y.; Wang, J.; Huang, X.; Ding, J. The Synthesis of Polypyrrole@Mn₃O₄/Reduced Graphene Oxide Anode with Improved Coulombic Efficiency. *Electrochim. Acta* **2015**, *186*, 345–352.
- (3) Seehra, M. S.; Geddam, U. K.; Schwegler-Berry, D.; Stefaniak, A. B. Detection and Quantification of 2H and 3R Phases in Commercial Graphene-Based Materials. *Carbon* **2015**, *95*, 818–823.
- (4) Shan, H.; Li, X.; Cui, Y.; Xiong, D.; Yan, B.; Li, D.; Lushington, A.; Sun, X. Sulfur/Nitrogen Dual-Doped Porous Graphene Aerogels Enhancing Anode Performance of Lithium Ion Batteries. *Electrochim. Acta* **2016**, *205*, 188–197.

- (5) Deerattrakul, V.; Limphirat, W.; Kongkachuichay, P. Influence of Reduction Time of Catalyst on Methanol Synthesis *via* CO₂ Hydrogenation Using Cu–Zn/N-rGO Investigated by In Situ XANES. *J. Taiwan Inst. Chem. Eng.* **2017**, *80*, 495–502.
- (6) Bin, Q.; Lin, B.; Zhu, K.; Shen, Y.; Man, Y.; Wang, B.; Lai, C.; Chen, W. Superior Trichloroethylene Removal from Water by Sulfide-Modified Nanoscale Zero-Valent Iron/Graphene Aerogel Composite. *J. Environ. Sci.* **2020**, *88*, 90–102.
- (7) Dong, S.; Cui, L.; Liu, C.; Zhang, F.; Li, K.; Xia, L.; Su, X.; Feng, J.; Zhu, Y.; Sun, J. Fabrication of 3D Ultra-Light Graphene Aerogel/Bi₂WO₆ Composite with Excellent Photocatalytic Performance: A Promising Photocatalysts for Water Purification. *J. Taiwan Inst. Chem. Eng.* **2019**, *97*, 288–296.
- (8) Ren, H.; Shi, X.; Zhu, J.; Zhang, Y.; Bi, Y.; Zhang, L. Facile Synthesis of N-Doped Graphene Aerogel and Its Application for Organic Solvent Adsorption. *J. Mater. Sci.* **2016**, *51*, 6419–6427.